arXiv:1611.04657v2 [physics.atom-ph] 24 Jan 2017

Electron-impact excitation of N^{3+} using the B-spline R-matrix method: Importance of the target structure description and the size of the close-coupling expansion.

L Fernández-Menchero, O Zatsarinny and K Bartschat

Department of Physics and Astronomy, Drake University, Des Moines IA, 50311, USA

Abstract.

There are major discrepancies between recent ICFT (Intermediate Coupling Frame Transformation) and DARC (Dirac Atomic R-matrix Code) calculations (Fernández-Menchero *et al.* 2014, *Astron. Astroph.* **566** A104, Aggarwal *et al.* 2016 *Mon. Not. R. Astr. Soc.* **461** 3997) regarding electron-impact excitation rates for transitions in several Be-like ions, as well as claims that the DARC calculations are much more accurate and the ICFT results might even be wrong. To identify possible reasons for these discrepancies and to estimate the accuracy of the various results, we carried out independent B-Spline R-Matrix (BSR) calculations for electron-impact excitation of the Be-like ion N^{3+}. Our close-coupling expansions contain the same target states (238 levels overall) as the previous ICFT and DARC calculations, but the representation of the target wave functions is completely different. We find close agreement among all calculations for the strong transitions between low-lying states, whereas there remain serious discrepancies for the weak transitions as well as for transitions to highly excited states. The differences in the final results for the collision strengths are mainly due to differences in the structure description, specifically the inclusion of correlation effects, rather than the treatment of relativistic effects or problems with the validity of the three methods to describe the collision. Hence there is no indication that one approach is superior to another, until the convergence of both the target configuration and the close-coupling expansions have been fully established.

PACS numbers: 34.50.Fa,52.20.Fs,95.30.Ky

Submitted to: *J. Phys. B: At. Mol. Phys.*

1. Introduction

Accurate and reliable electron-impact excitation data are required for the modeling and spectroscopic diagnostics of various non-equilibrium astrophysical and laboratory plasmas. Emission lines from beryllium-like ions (in particular N^{3+}) are used for electron density and temperature diagnostics for a variety of emission sources. Many references and examples are given in previous publications on Be-like ions [1, 2]. For the processes of interest here, the Be-like ions can be modeled well as two-electron systems with a frozen $1s^2$ core. Despite the simple structure of these ions, the electron-impact collision strengths from recent calculations [1, 2] differ considerably. This calls for additional analysis of the methods used to obtain these results, as well as the existing data.

Many formulations and the associated computer codes have been developed to treat electron scattering from atoms and ions. The most frequently applied *general* approach is the R-matrix method developed by Burke and collaborators over the past decades. The basic ideas, as well as numerous applications and extensions to other fields and processes, are described in [3]. The suite of Belfast R-matrix codes [4] (see, for example, [5] for updates) is, within the usual computational restraints, applicable to the calculation of electron (and photon) induced processes for any atomic or ionic target. Relativistic corrections, which are only expected to be important for heavy targets, are often included through the Breit-Pauli approximation. An alternative and, in principle, more satisfactory approach is to use the Dirac-Coulomb hamiltonian, as implemented in the full-relativistic Dirac Atomic R-matrix Code (DARC) [6]. However, even for the significantly heavier (than N^{3+}) target Fe^{14+} only small differences between Dirac-Coulomb and Breit-Pauli results were found in a detailed comparison study [7], provided the target structure description was similar in the two calculations. Hence, it is very unlikely that the semi-relativistic Breit-Pauli approach is insufficient for a light system such as N^{3+} regarding the treatment of relativistic effects in generating data for practical modeling applications.

Like most standard implementations of atomic structure and collision codes, the above-mentioned suites of programs employ a fixed set of mutually orthogonal one-electron orbitals for *all* states included in the expansion of the total wave function. In addition, the orbitals employed for the description of the projectile are made orthogonal to those used in the target description. These choices are due to technical rather than physical reasons. (Note that only the multi-electron wave functions of the same symmetry and different total energies have to be orthogonal, but not the individual one-electron orbitals.) A significant advantage of the above choice is a simplification in setting up the hamiltonian matrix. On the other hand, these restrictions limit the flexibility in the description of the target structure.

The present calculations were carried out with a parallelized version of the B-spline Breit-Pauli R-matrix (BSR) code [8]. A distinct feature of the method (see [9] for a comprehensive overview) is the use of term-dependent non-orthogonal orbital sets in the description of the target states. This allows us to optimize the wave functions for different states independently, thereby resulting in a more accurate target description than those used in previous collision calculations. The BSR code has been primarily applied to electron scattering from neutral atoms [9], where electron correlation effects are most important and an accurate representation of the target states becomes a primary task. It has also been applied to electron collisions with multi-charged ions, including Fe^{6+} [10] and Fe^{7+} [11]. Both of these ions have a complicated structure with open 3p and 3d subshells, and an accurate representation of the target states even for these highly-charged ions is not a trivial task. The distinct feature of the above calculations was a careful analysis of the convergence of the CI expansions for the target states.

The semi-relativistic (Breit-Pauli) or full-relativistic (Dirac-Coulomb) approaches require much more computational effort than non-relativistic calculations. An alternative to a full Breit-Pauli R-matrix calculation for electron-impact excitation is the algebraic transformation of the scattering ($\boldsymbol{S}$) or reactance ($\boldsymbol{K}$) matrices, first calculated in pure LS-coupling, to a relativistic coupling scheme. In particular, Griffin *et al.* [12] introduced the intermediate-coupling frame transformation (ICFT) method, which employs multi-channel quantum defect theory (MQDT). Even though the spin-orbit interaction between the colliding electron and the target is neglected in the ICFT approach, it turned out to be a very accurate approximation to the direct Breit-Pauli approach. Numerous calculations [13, 14] showed that the differences observed between the ICFT and the other R-matrix results are well within the uncertainties to be expected due to the use of different target descriptions or different close-coupling (CC) expansions for the scattering electron. At the same time, the ICFT method is computationally much more effective and has been applied in systematic calculations for entire isoelectronic sequences.

Fernández-Menchero *et al.* [1] performed extensive

R-matrix ICFT calculations for the Be-like isoelectronic sequence up to Kr^{32+}, including N^{3+}. For the latter, their scattering model included 238 intermediate-coupling (IC) levels. Later, Aggarwal and coworkers published 98-level R-matrix calculations obtained with the DARC code for the Be-like ion Al^{9+} [15] and a 166-level calculation for C^{2+} [16]. The differences in the obtained collision rates compared to the ICFT results of [1] led Aggarwal *et al.* to cast doubt on the validity of the ICFT approach in general and/or the practical implementation. Fernandez-Menchero [13], however, showed that the different results were simply due to variations in the description of the target structure among the calculations. Similar criticism of ICFT was put forward by Aggarwal *et al.* regarding the ion Fe^{13+} [17], but their arguments were again rebutted by Del Zanna *et al*. [14].

Recently, new calculations for the Be-like ion N^{3+} appeared [2], this time also obtained from a 238-level expansion with the same set of configurations as used in [1]. Since, once again, differences were found, the question remains whether these are mainly due to the treatment of the collision part of the problem or the still different structure descriptions of the 238 target states.

The principal motivation for the present work, therefore, was to shed more light on the ongoing discussion by performing an independent calculation for electron collisions with N^{3+}. We use the BSR approach, which employs entirely different numerical methods for both the target states and the collision calculations. For a proper comparison of the results, we select the same set of target states in the CC expansion as in previous ICFT [1] and DARC [2] calculations. This allows us to directly draw conclusions regarding the sensitivity of the predictions to the target structure description in the case of interest. Furthermore, we note that the BSR approach is expected to have the most accurate representation of the target states, due to its flexibility in employing term-dependent, individually optimized, and hence non-orthogonal one-electron orbitals.

This manuscript is organized as follows. In Sect. 2 we describe the structure calculations. This is followed with some details about the close-coupling expansion in Sect. 3, where we also summarize the way to obtain the collision strength Ω and the effective collision strength Υ. Our results are presented and discussed in Sect. 4, and the conclusions are summarized in Sect. 5. Unless specified otherwise, atomic units are used throughout.

2. Structure Model

The target states of N^{3+} in the present calculations were generated using the B-spline box-based close-coupling method [18, 19]. Relativistic effects were accounted for at the level of the Breit-Pauli approximation in the intermediate-coupling scheme. Specifically, the structure of the multichannel target expansions for states with given total electronic angular momentum J and parity was chosen as

$$\begin{aligned}\Phi^{2lnl,J} = &\sum_{nl,LS} a_{nl}^{LS\,J}\{\phi(2s)\,P_{nl}\}^{LS} + \sum_{nl,LS} b_{nl}^{LS\,J}\{\phi(2p)\,P_{nl}\}^{LS} \\ &+ \sum_{nl,LS} c_{nl}^{LS\,J}\{\phi(3s)\,P_{nl}\}^{LS} + \sum_{nl,LS} d_{nl}^{LS\,J}\{\phi(3p)\,P_{nl}\}^{LS} \\ &+ \sum_{nl,LS} e_{nl}^{LS\,J}\{\phi(3d)\,P_{nl}\}^{LS}\,. \end{aligned} \quad (1)$$

Here ϕ denotes the Hartree-Fock (HF) functions of the three-electron $1s^2nl$ ionic states, with the core 1s orbital frozen; P_{nl} denotes the wave function of the outer valence electron, and $\{\}$ stands for an antisymmetrized product of functions, conserving the total orbital angular momentum L and the spin S. The above expansion is similar to the one used in our recent calculations for electron scattering from neutral Be [20]. Usually we employ separate multi-configuration Hartree-Fock (MCHF) expansions for a more accurate representation of the low-lying states with equivalent electrons, in particular $2s^2$ and $2p^2$ in the present case. However, we found that these states are already represented accurately by the expansions (1) alone, and hence the expansions for N^{3+} could be simplified in comparison to those for neutral Be. Bearing in mind that the final multi-configuration expansions still need to be dealt with in the subsequent collision calculation with one more electron to be coupled in, such simplification is very helpful from a computational point of view.

The unknown radial functions $P_{nl}(r)$ for the outer valence electron were expanded in a B-spline basis

$$P_{nl}(r) = \sum_k c_k\,B_k(r)\,, \quad (2)$$

where $B_k(r)$ denotes an individual B-spline. The coefficients c_k for each valence orbital $P_{nl}(r)$, as well as the various coefficients in Eq. (1) were obtained by diagonalizing the N-electron target hamiltonian, including all one-electron Breit-Pauli corrections. The corresponding equations were solved subject to the condition that the wave functions vanish at the boundary. The number of spectroscopic bound states that can be generated in the above scheme depends on the B-spline box radius. In the present calculations, this radius was set to $40\,a_0$, where $a_0 = 0.529 \times 10^{-10}$ m is the Bohr radius. The expansion (2) included 134 B-splines of order 8, with the step h between the knots varying from 0.125 to $0.4\,a_0$. This allowed us to obtain accurate descriptions of the N^{3+} states with principal quantum number for the valence electron up to $n = 7$. Note that the above B-spline bound-state close-coupling calculations generate different non-orthogonal sets of one-electron orbitals for each target state, and hence their subsequent use is somewhat complicated. Our configuration expansions contained between 10 and 50 configurations for each state and could still be used

Table 1. The lowest 40 energy Levels of N^{3+}.

i	Conf	Level	NIST	BSR (%)	GRASP (%)	AS (%)	τ
1	$2s^2$	$^1S^e_0$	0.0	0.0 (–)	0.0 (–)	0.0 (–)	stable
2	2s 2p	$^3P^o_0$	67209.2	67388.1 (0.3)	67811.1 (0.9)	68401.0 (1.8)	stable
3	2s 2p	$^3P^o_1$	67272.3	67458.7 (0.3)	67870.3 (0.9)	68485.0 (1.8)	2.070 [−3]
4	2s 2p	$^3P^o_2$	67416.3	67600.5 (0.3)	68008.6 (0.9)	68655.0 (1.8)	8.590 [+1]
5	2s 2p	$^1P^o_1$	130693.9	132950.2 (1.7)	138128.6 (5.7)	138278.0 (5.8)	4.060 [−10]
6	$2p^2$	$^3P^e_0$	175535.4	177326.3 (1.0)	178454.8 (1.7)	179729.0 (2.4)	5.360 [−10]
7	$2p^2$	$^3P^e_1$	175608.1	177396.9 (1.0)	178524.0 (1.7)	179813.0 (2.4)	5.360 [−10]
8	$2p^2$	$^3P^e_2$	175732.9	177536.5 (1.0)	178639.2 (1.7)	179979.0 (2.4)	5.350 [−10]
9	$2p^2$	$^1D^e_2$	188882.5	190712.2 (1.0)	195946.9 (3.7)	197490.0 (4.6)	4.380 [−9]
10	$2p^2$	$^1S^e_0$	235369.3	241108.7 (2.4)	247825.3 (5.3)	248501.0 (5.6)	3.020 [−10]
11	2s 3s	$^3S^e_1$	377284.8	376494.3 (−0.2)	375937.0 (−0.4)	374017.0 (−0.9)	1.120 [−10]
12	2s 3s	$^1S^e_0$	388854.6	388219.7 (−0.2)	387760.1 (−0.3)	386213.0 (−0.7)	4.090 [−10]
13	2s 3p	$^1P^o_1$	404522.4	403910.7 (−0.2)	404057.2 (−0.1)	402317.0 (−0.5)	7.760 [−11]
14	2s 3p	$^3P^o_0$	405971.6	405292.5 (−0.2)	404875.8 (−0.3)	403110.0 (−0.7)	8.290 [−9]
15	2s 3p	$^3P^o_1$	405987.5	405310.3 (−0.2)	404891.2 (−0.3)	403128.0 (−0.7)	8.040 [−9]
16	2s 3p	$^3P^o_2$	406022.8	405344.8 (−0.2)	404925.2 (−0.3)	403161.0 (−0.7)	8.230 [−9]
17	2s 3d	$^3D^e_1$	420045.8	419102.3 (−0.2)	419130.7 (−0.2)	417332.0 (−0.6)	3.300 [−11]
18	2s 3d	$^3D^e_2$	420049.6	419109.5 (−0.2)	419134.0 (−0.2)	417339.0 (−0.6)	3.300 [−11]
19	2s 3d	$^3D^e_3$	420058.0	419120.3 (−0.2)	419142.8 (−0.2)	417350.0 (−0.6)	3.300 [−11]
20	2s 3d	$^1D^e_2$	429159.6	428645.9 (−0.1)	430447.9 (0.3)	428315.0 (−0.2)	5.420 [−11]
21	2p 3s	$^3P^o_0$	465291.8	464987.9 (−0.1)	465023.9 (−0.1)	463467.0 (−0.4)	1.460 [−10]
22	2p 3s	$^3P^o_1$	465371.0	465066.2 (−0.1)	465101.9 (−0.1)	463552.0 (−0.4)	1.460 [−10]
23	2p 3s	$^3P^o_2$	465536.6	465226.9 (−0.1)	465263.2 (−0.1)	463725.0 (−0.4)	1.450 [−10]
24	2p 3s	$^1P^o_1$	473029.3	472983.1 (−0.0)	474725.8 (0.4)	473301.0 (0.1)	1.200 [−10]
25	2p 3p	$^1P^e_1$	480884.2	480661.1 (−0.0)	480548.5 (−0.1)	478848.0 (−0.4)	1.290 [−10]
26	2p 3p	$^3D^e_1$	484498.2	484323.7 (−0.0)	484764.6 (0.1)	482889.0 (−0.3)	2.750 [−10]
27	2p 3p	$^3D^e_2$	484594.9	484419.2 (−0.0)	484861.2 (0.1)	482988.0 (−0.3)	2.760 [−10]
28	2p 3p	$^3D^e_3$	484746.2	484567.3 (−0.0)	485010.4 (0.1)	483142.0 (−0.3)	2.750 [−10]
29	2p 3p	$^3S^e_1$	487607.4	487167.3 (−0.1)	487384.0 (−0.0)	485622.0 (−0.4)	9.980 [−11]
30	2s 4s	$^1S^e_0$	–	494216.6 (–)	493653.3 (–)	492046.0 (–)	5.410 [−10]
31	2p 3p	$^3P^e_0$	494253.1	494474.0 (0.0)	494289.8 (0.0)	493059.0 (−0.2)	1.920 [−10]
32	2p 3p	$^3P^e_1$	494309.2	494511.4 (0.0)	494334.8 (0.0)	493110.0 (−0.2)	1.860 [−10]
33	2p 3p	$^3P^e_2$	494402.0	494607.6 (0.0)	494422.6 (0.0)	493217.0 (−0.2)	1.860 [−10]
34	2p 3d	$^3F^o_2$	495406.2	494807.6 (−0.1)	495606.6 (0.0)	494003.0 (−0.3)	1.830 [−8]
35	2p 3d	$^3F^o_3$	495482.6	494884.7 (−0.1)	495680.2 (0.0)	494087.0 (−0.3)	2.040 [−8]
36	2p 3d	$^3F^o_4$	495585.7	494986.6 (−0.1)	495777.8 (0.0)	494196.0 (−0.3)	2.110 [−8]
37	2s 4s	$^3S^e_1$	498045.5	497406.9 (−0.1)	497108.9 (−0.2)	495026.0 (−0.6)	2.320 [−9]
38	2p 3d	$^1D^o_2$	498310.3	497915.1 (−0.1)	497699.3 (−0.1)	496164.0 (−0.4)	7.200 [−11]
39	2p 3p	$^1D^e_2$	499705.9	499803.8 (0.0)	501828.7 (0.4)	500670.0 (0.2)	1.030 [−10]
40	2s 4p	$^3P^o_2$	503680.4	502965.3 (−0.1)	502495.9 (−0.2)	500770.0 (−0.6)	1.820 [−10]

Key: i, level index; Conf, Level: Configuration and multiplet, largest weight; BSR: calculated excitation energy relative to the ground state, present work; NIST: recommended value from the NIST data base [24]; AS: work [1]. GRASP: work [2]; %: relative deviation with respect to the recommended values; τ: life-time (in seconds), present work. All energies are given in cm^{-1}. $A\,[B]$ denotes $A \times 10^B$.

in the collision calculations with moderate computational resources.

Standard R-matrix calculations employ CI expansions of the target states based on a single set of orthogonal one-electron radial functions [3]. The ICFT calculations for Be-like ions [1], for example, used atomic levels generated by `AUTOSTRUCTURE` (AS) [21], with the 1s to 7d orbitals obtained from a Thomas-Fermi-Dirac-Amaldi model potential with optimized scaling parameters. These CI expansions included the configuration $1s^2\{2s^2, 2s2p, 2p^2\}$ and all $1s^2\{2s, 2p\}nl$ configurations with $n = 3-7$ and $l = 0-5$ for $n = 3-5$ and $l = 0-2$ for $n = 6, 7$. The DARC calculation [2] used orbitals obtained with the GRASP (General-purpose Relativistic Atomic Structure Package) program [22, 23] in the "extended average level" approximation. Those CI expansions included the same set of configurations, albeit in the jj-coupling scheme.

Note that Eq. (1) is not just a minimal CI expansion, but it is enlarged by the inclusion of all 2snl, 2pnl, 3snl, 3pnl and 3dnl configurations, respectively, where nl are the physical bound orbitals as well as the pseudo-orbitals that are used to discretize the continuum. Consequently, we include all important single and double promotions for the 2snl and 2pnl states under consideration. This is very important for an accurate description of the valence correlation between the two outer electrons above the $1s^2$ core. Furthermore, we directly include the term dependence of the one-electron wave functions. This term dependence

is well known to be important for neutral Be, and it may be significant for other Be-like ions as well.

The expansion (1) generates an extensive spectrum of the N^{3+} ionic target, including the continuum. This spectrum was reduced in the present calculations by limiting the maximum total electronic angular momentum to $J = 6$. Altogether, we obtained 1400 bound and continuum levels of N^{3+}. From these we selected for the close-coupling expansion just the same 238 levels as in the previous works [1, 2].

In Table 1 we list the excitation energies calculated with the BSR method for the lowest 40 levels. We compare them with the AS and GRASP results [1, 2], as well as the recommended values tabulated in the NIST database [24]. (The complete table of states can be found in the supplemental online material.) As seen from the tables, our excitation energies agree much closer with experiment than either the AS or GRASP energies, especially for the low-lying $n = 2$ states. This is due to the more extensive CI expansions in our approach. As noted in [2], there is room for improving the accuracy of the energy levels by including pseudo-orbitals in the target wave functions, but it may lead to pseudo-resonance structure in the final collision strengths [3]. Therefore, both Aggarwal *et al.* [2] and Fernandez-Menchero *et al.* [1] avoided this approach. The present BSR calculation, due to the use of non-orthogonal orbitals for both the bound and continuum spectrum, is free from these restrictions.

Table 2 shows the upper part of the spectrum to illustrate how the states included are embedded into the full spectrum. Above level #87 ($2s\,6d\,^3D_3$), there are levels (e.g., $2s\,6\{f, g, h\}$) that are not found in the CI or CC expansions of [1, 2]. Since the close-lying states may be strongly mixed, the expansions of [1] and [2] neglect possibly important contributions to the wave functions in all levels above #87. In addition, the $2pnl$ states, starting at the multiplet $2p5s\,^3P^o$, are located above the ionization threshold and hence are expected to strongly interact with the $2skl$ continuum. Our expansions (1) include these interactions through the continuum pseudostates, whereas they are completely omitted in the CI expansions used in [1, 2].

A standard assessment regarding the quality of structure calculations involves a comparison of the oscillator strengths f, or the closely related gf, which is the value of f multiplied by the statistical weight $(2J + 1)$ of the initial level. The gf-values are the same for excitation and de-excitation. Note that oscillator strengths themselves are also very important for plasma modeling.

We begin by comparing results for the transitions between the lowest 20 states, where there are numerous data from other calculations. In particular, Froese-Fischer and coworkers [25] presented extensive MCHF calculations with a large set of configurations and a careful analysis of convergence. It is generally accepted that this work

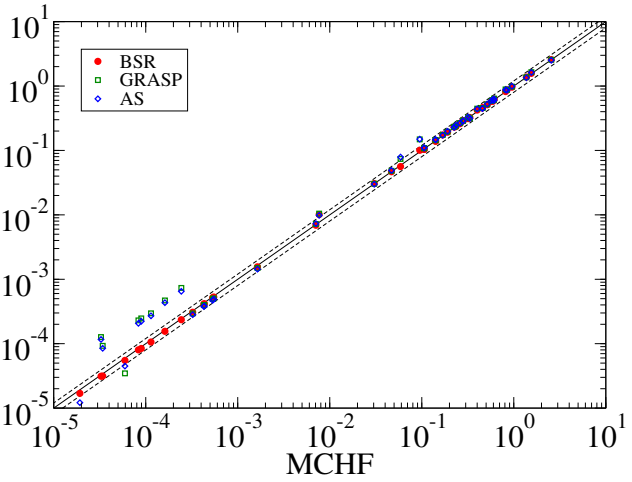

Figure 1. Comparison of gf from the BSR, DARC, and AS calculations with the MCHF results [25]. x-axis: gf results for a certain transition calculated with the MCHF method [25]; y-axis: gf results for the same transition calculated with BSR (present work), GRASP [2], and AS [1]. The dashed lines show the bands corresponding to a 20% deviation from the MCHF results.

represents the most accurate calculation for the structure of the lowest excited levels of several Be-like ions, including N^{3+}. Figure 1 shows a comparison of the MCHF oscillator strengths with the results from the BSR, DARC, and AS models for transitions between the lowest 20 levels. We see very good agreement between the BSR and MCHF results for all transitions, including the very weak ones with small gf-values. This suggests similarly accurate configuration mixing in both calculations. The DARC and AS results only show good agreement with MCHF for strong transitions with gf-values larger than 10^{-3}, whereas they differ considerably from MCHF and BSR for weak transitions, where configuration mixing plays an important role. This mixing primarily depends on correlation corrections, included in the MCHF and BSR calculations, rather than on the spin-orbit mixing that is accounted for in all models.

Only a few experimental data for the oscillator strengths or transition rates in N^{3+} are available to assess the accuracy of the different predictions independently of the MCHF results. Table 3 shows a comparison with experiment for the two lines from the 2s2p configuration. For the strong resonant $2s^2\,^1S_0 - 2s2p\,^1P^o_1$ transition all calculations agree closely with each other and with experiment. For the weak intercombination transition $2s^2\,^1S_0 - 2s2p\,^3P^o_1$, the agreement is not close, and the presumably best model (MCHF) produces a value that deviates from experiment by more than twice the estimated experimental uncertainty. Note, however, that the relative experimental uncertainty is large (more than 25%). Hence, while the GRASP number appears to agree best with the experimental result, the BSR prediction deviates from the latter by just about the published uncertainty and hence

Table 2. Selected high-lying energy levels of N^{3+}.

i	Conf.	Level	NIST	BSR (%)	GRASP (%)	AS (%)
85	2s 6d	$^3D^e_1$	575030.5	573968.2 (−0.2)	573321.5 (−0.3)	571523.0 (−0.6)
86	2s 6d	$^3D^e_2$	575030.5	573969.0 (−0.2)	573321.5 (−0.3)	571524.0 (−0.6)
87	2s 6d	$^3D^e_3$	575030.5	573970.3 (−0.2)	573322.6 (−0.3)	571525.0 (−0.6)
88	2s 6g	$^3G^e_3$	575809.4	574725.8 (−0.2)	–	–
89	2s 6g	$^3G^e_4$	575809.4	574726.4 (−0.2)	–	–
90	2s 6g	$^1G^e_4$	575807.9	574728.2 (−0.2)	–	–
91	2s 6g	$^3G^e_5$	575809.4	574728.2 (−0.2)	–	–
92	2s 6f	$^3F^o_2$	–	574842.5	–	–
93	2s 6f	$^3F^o_3$	–	574843.4	–	–
94	2s 6f	$^3F^o_4$	–	574844.7	–	–
95	2s 6d	$^1D^e_2$	575872.4	574867.5 (−0.2)	574527.5 (−0.2)	572601.0 (−0.6)
96	2s 6f	$^1F^o_3$	575999.3	574924.7 (−0.2)	–	–
97	2s 6h	$^3H^o_4$	576042.9	574956.5 (−0.2)	–	–
98	2s 6h	$^3H^o_5$	576042.9	574956.6 (−0.2)	–	–
99	2s 6h	$^1H^o_5$	576042.9	574956.8 (−0.2)	–	–
100	2s 6h	$^3H^o_6$	576042.9	574956.8 (−0.2)	–	–
101	2p 4s	$^3P^o_0$	577957.8	577512.3 (−0.1)	577188.6 (−0.1)	575628.0 (−0.4)
102	2p 4s	$^3P^o_1$	578045.4	577589.6 (−0.1)	577267.7 (−0.1)	575712.0 (−0.4)
266	2s 11d	$^3D^e_3$	610166.0	620383.2 (1.7)	–	–
267	2s 11d	$^1D^e_2$	610287.2	620914.7 (1.7)	–	–
268	2s 12k	$^3K^o_6$	–	622346.8	–	–
Ionization limit			624866.0			
269	2s ki	$^3I^e_5$	–	624777.0	–	–
270	2s ki	$^3I^e_6$	–	624777.0	–	–
271	2s ki	$^1I^e_6$	–	624777.1	–	–
272	2p 5s	$^3P^o_0$	626355.0	625844.3 (−0.1)	625435.8 (−0.1)	623873.0 (−0.4)
273	2p 5s	$^3P^o_1$	626445.3	625915.4 (−0.1)	625511.5 (−0.1)	623952.0 (−0.4)
274	2p 5s	$^3P^o_2$	626611.9	626089.6 (−0.1)	625684.9 (−0.1)	624133.0 (−0.4)
275	2p 5s	$^1P^o_1$	628546.9	627025.1 (−0.2)	627423.1 (−0.2)	625792.0 (−0.4)

Key: i, level index; Conf., Level: Configuration and multiplet, largest weight; BSR: calculated excitation energy relative to the ground state, present work; NIST: recommended value from the NIST data base [24]; AS [1]. GRASP [2]; %: relative deviation from the recommended values. All energies are given in cm^{-1}.

is essentially consistent with experiment as well. This clearly shows that theoretical results for weak transitions are very sensitive to the model employed, due to the increasing likelihood of cancellations from contributing matrix elements. Experimental data for such transitions are generally uncertain as well. Based on long-term experience in extensive structure calculations, we continue to believe that the MCHF result is the most reliable, due to the size of the expansion and the systematic convergence checks performed. Unfortunately, only an independent experiment and/or even more extensive structure calculations, using as much as possible similar semi-relativistic and full-relativistic expansions, would be able to shed more light on this problem.

For further comparison of the present target structure with previous works, we show in Fig. 2 the gf-values of BSR vs. DARC and ICFT for the electric dipole-allowed transitions between all 238 IC levels included in the scattering calculations. (A complete list of the radiative parameters from the present BSR calculations is provided in the online supplemental material.) The differences in the gf-values are relatively small, on average less than 50%, for most transitions with an upper level up to #87. There are a few exceptions for weak transitions, where the differences can be as large as several orders of magnitude. In these cases, the electric dipole transition takes place through spin-orbit mixing between configurations of small weight in the

Table 3. Comparison of oscillator strengths and transition rates.

$2s^2\,^1S_0 - 2s2p\,^1P^o_1$	f-factor
Present work	0.6268
Expt. [26]	0.620 ± 0.022
MCHF [25]	0.610
GRASP [2]	0.6391
AS [1]	0.6326

$2s^2\,^1S_0 - 2s2p\,^3P^o_1$	Transition rate A (s^{-1}).
Present work	4.772×10^{-7}
Expt. [27]	$(3.8 \pm 0.9) \times 10^{-7}$
MCHF [25]	5.755×10^{-7}
GRASP [2]	4.030×10^{-7}
AS [1]	5.781×10^{-7}

CI expansion. A slight change in the mixing coefficients can then change the gf-value considerably. In practice, an accurate description of such weak intercombination transitions can only be achieved in specially designed calculations, with careful consideration of each individual transition. However, since such transitions usually have very small gf-values, they are unlikely to have a significant effect in plasma modeling.

As seen from Fig. 2, the differences in the gf-values obtained by the various methods considerably increase for levels above #87. This applies to both the BSR/DARC and BSR/AS comparisons, with approximately the same level of agreement or disagreement. Note that the BSR expansions for these levels are very different from those used in the DARC and AS calculations. They are more extensive and include configuration mixing with the additional $\{3s, 3p, 3d\}nl$ bound states, as well as the interaction with the continuum (see Table 2).

As a result, the spin-orbit mixing is also described very differently for these states. These differences in the gf-values are expected to cause deviations of the same order in the final results for the effective collisions strength Υ, especially at high temperatures. To illustrate the effect of the different relativistic approaches on the predicted target structure, we show in Fig. 3 the same gf-values, but this time limited to spin-conserving transitions. Relativistic effects, specifically the spin-orbit interaction, should be negligible in these cases. Since the dispersion seen in the figure for spin-conserving transitions is similar to that for the spin-changing ones, the way to include relativistic terms in the hamiltonian affects to a much lesser extent the predicted target properties than the method used to expand the wave functions.

Variations in the f-values also results in different predictions of the lifetimes. A comparison of lifetimes from the various calculations is shown in Fig. 4. The ratios of the MCHF, DARC, and AS results to the BSR predictions are close to 1 for the low-lying states, but they differ considerably for some states in the upper-part of the spectrum. This indicates, once more, the sensitivity of the results to the different configuration expansions used in the individual methods. Since it is unlikely that the configuration expansions are near convergence in either the DARC or the AS calculations, the accuracy of the predicted collision strengths from these models is questionable. This will be further discussed below.

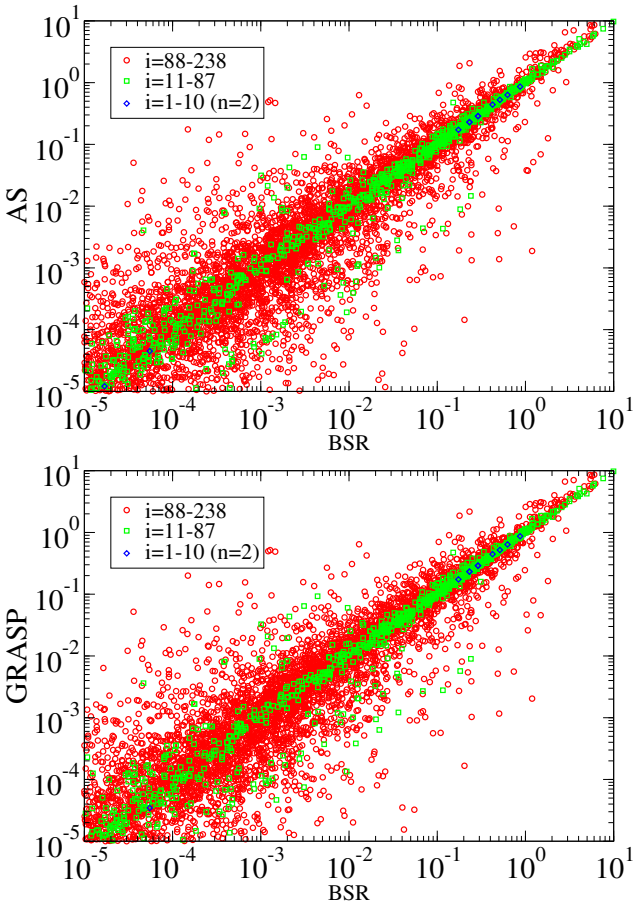

Figure 2. Comparison of gf-values for the N^{3+} structure obtained in the present work with [1] (top panel) and [2] (bottom panel). x-axis: gf results for a certain transition calculated with the BSR method, present work; y-axis: gf results for the same transition calculated with AS (upper panel [1]) and GRASP (lower panel [2]). $\diamond$: transitions within the $n = 2$ electronic shell, upper level up to 10; $\square$: transitions with upper level between 11 and 87; $\circ$: transitions with upper level above 88.

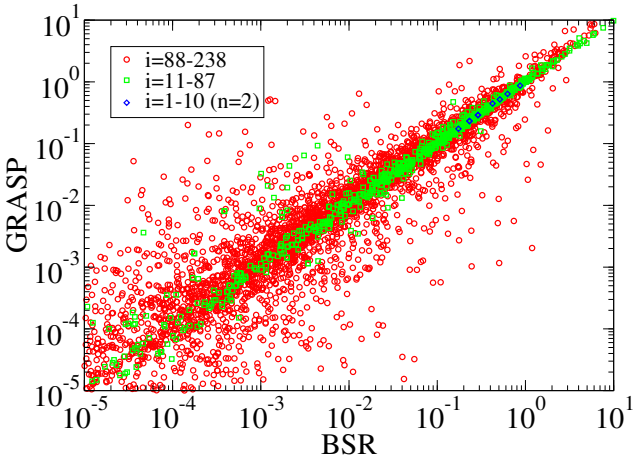

Figure 3. As in Fig. 2, but limited to spin-conserving transitions.

3. Collision Calculations

For the scattering calculations we used the B-spline R-matrix code of Zatsarinny [8]. The distinctive feature of the method is the use of B-splines as a universal basis to represent the scattering orbitals in the inner region of $r \leq a$. The principal advantage of B-splines is that they form an effectively complete basis, and hence no Buttle

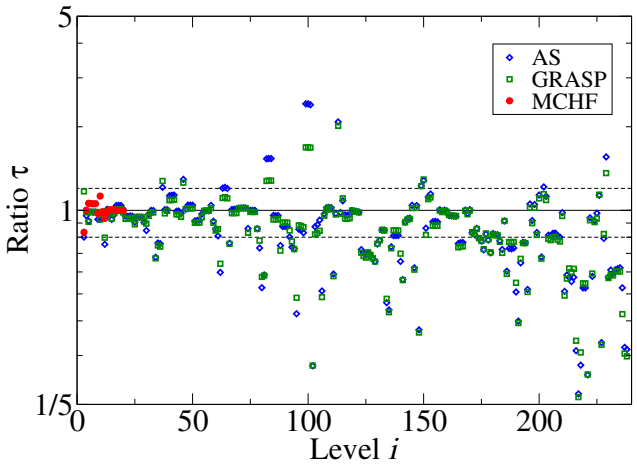

Figure 4. Lifetimes from the MCHF, DARC, and AS calculations normalized to the BSR predictions. The dashed lines indicate the band of 20% deviation. ⋄: τ(AS)/τ(BSR); □: τ(GRASP)/τ(BSR); •: τ(MCHF)/τ(BSR).

correction [3, 30] to the R-matrix is needed in this case. The amplitudes of the wave functions at the boundary, which are required for the evaluation of the R-matrix, are given by the coefficient of the last spline, which is the only spline with nonzero value at the boundary.

The other important feature of the present code concerns the orthogonality requirements for the one-electron radial functions. We impose only limited orthogonality conditions on the continuum orbitals. This avoids the $(N+1)$-electron bound-like configurations, which need to be included in standard R-matrix calculations to ensure the numerical completeness of the expansion [3]. It also allows us to use much more extensive multi-configuration expansions for the target states while avoiding the pseudo-resonance structure that may appear in calculations with an extensive number of correlated orbitals.

The present close-coupling expansions include 238 target states, the same ones as in [1, 2]. These states consist of all LSJ levels arising from the configurations $1s^2\,\{2s^2, 2s\,2p, 2p^2\}$ and $1s^2\,\{2s, 2p\}\,nl$ for nl orbitals 3s, 3p, 3d, 4s, 4p, 4d, 4f, 5s, 5p, 5d, 5f, 5g, 6s, 6p, 6d, 7s, 7p, 7d. Relativistic effects in the scattering calculations were incorporated via the Breit-Pauli hamiltonian through the one-electron Darwin, mass correction, and spin-orbit operators. The computing resources needed in this approach are about an order of magnitude larger than in the ICFT formalism, due to the size of the hamiltonian matrices that need to be diagonalized. In [1] the CC calculation was carried out in LS-coupling with only 130 terms, and afterwards the $\boldsymbol{K}$-matrixes were recoupled to obtained the level-resolved collision strengths.

In the inner region, we used the same B-spline set as for the target CI structure described in Sect. 2. Numerical calculations were performed for 90 LSJ partial waves up to $J_{\max} = 89/2$, for both even and odd parities. The maximum number of channels in a partial wave was 1116, the maximum number of physical and correlated orbitals was 4837, and the maximum number of configurations was 83095. To account for the contributions from angular momenta higher than $J_{\max} = 89/2$, we used the Burgess sum rule [31] for optically allowed transitions and a geometric series for all others [32].

For the outer region we employed a parallel version of the PSTGF program [33, 34]. In the resonance regime for impact energies below the excitation energy of the highest level included in the CC expansion, we used a fine energy step of $10^{-5}\,z^2$ Ry, with $z = 3$ as the target ionic charge, to properly map those resonances. For energies above the highest excitation threshold included in the CC expansion, the collision strengths vary smoothly, and hence we chose a coarser step of $10^{-2}\,z^2$ Ry. Altogether, 61279 energies for the colliding electron were considered. We calculated collision strengths up to 30 Ry, which is about five times the ionization potential of N^{3+} [24]. For even higher energies we extrapolated using the well-known asymptotic energy dependence for the various transitions. To obtain effective collision strengths $\Upsilon(T)$, we convoluted Ω with a Maxwellian distribution for the electron temperature T, i.e.,

$$\Upsilon_{i-j}(T) = \int_{E_{th}}^{\infty} \mathrm{d}E\,\Omega_{i-j}(E)\,\exp\left(\frac{E-E_{th}}{kT}\right). \qquad (3)$$

Here E_{th} is the $i-j$ transition energy and k is the Boltzmann constant.

4. Results and Discussion

Figure 5 exhibits the resonance structure of the collision strength Ω for three selected transitions, one dipole-allowed with spin-change $(1-3)$, one M1−E2 with spin-change $(3-5)$ and finally a one-photon forbidden double-electron jump $(1-10)$. These results are from the present BSR calculation and a previous ICFT model [1]. DARC results for the same transitions are shown in [2]. The resonance structure looks similar for these three transitions in BSR and ICFT, while in the figures of [2] there are some prominent features in the transitions $3-5$ and $1-10$ between 4.5 and 5.5 Ry, respectively. They are very narrow, however, and do not contribute significantly to the effective collision strengths Υ, which are shown in Fig. 6 along with the strong dipole transition $1-5$. Results for the Υs agree very closely, to within 20%, over a wide range of temperatures, except for the spin-changing transition $1-3$ $2s^2\,{}^1S_0 - 2s2p\,{}^3P_1$ where Υ decreases at low temperatures in the ICFT calculations. This can be due to the position or the resolution of the resonances, as will be discussed below.

Figure 7 shows a global comparison of the effective collision strengths obtained previously [1, 2] at three different temperatures. The dispersions at all three temperatures are similar to those seen in the gf-factors in Fig. 2. This confirms that the target structure is the

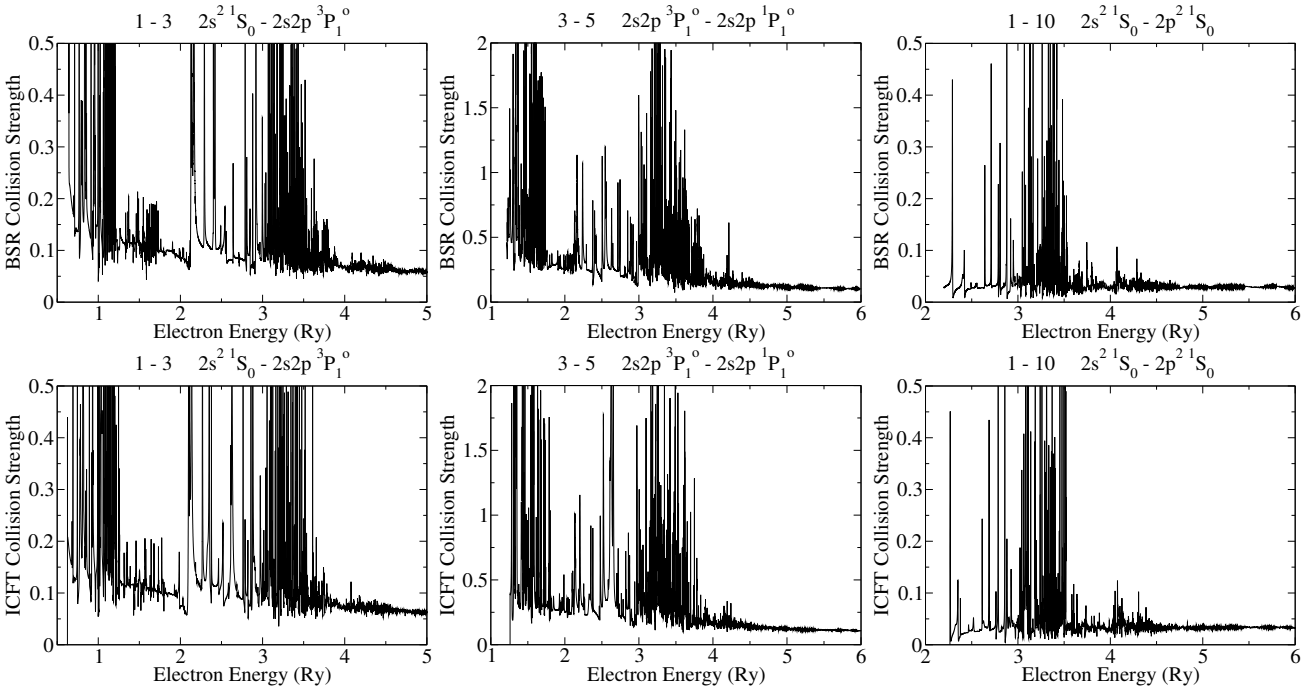
1 - 3 2s² ¹S₀ - 2s2p ³P₁°
3 - 5 2s2p ³P₁° - 2s2p ¹P₁°
1 - 10 2s² ¹S₀ - 2p² ¹S₀
BSR Collision Strength
ICFT Collision Strength
Electron Energy (Ry)

Figure 5. Collision strength Ω for electron-impact excitation of N^{3+} for selected transitions. Top panels: present BSR; bottom panels: ICFT [1].

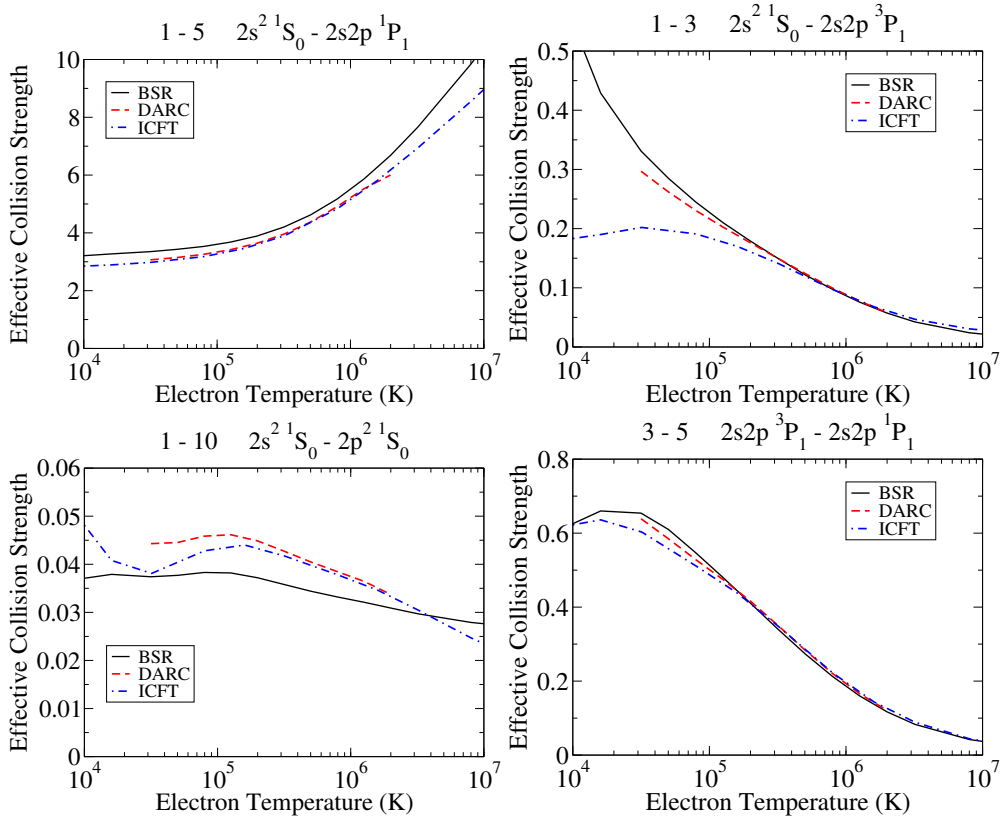
1 - 5 2s² ¹S₀ - 2s2p ¹P₁
1 - 3 2s² ¹S₀ - 2s2p ³P₁
1 - 10 2s² ¹S₀ - 2p² ¹S₀
3 - 5 2s2p ³P₁ - 2s2p ¹P₁
BSR
DARC
ICFT
Effective Collision Strength
Electron Temperature (K)

Figure 6. Electron-impact excitation effective collision strengths versus electron temperature for N^{3+} for some selected transitions. Solid line: present work; dashed line: [2]; dash-dotted line: [1].

Table 4. Number of transitions in the upper panels of Fig. 7 that differ by more than $\delta = |\Upsilon_{\rm DARC} - \Upsilon_{\rm BSR}|/\Upsilon_{\rm BSR}$.

δ		Temperature (K)		
(%)	gf	3.2×10^4	1.6×10^5	1.6×10^6
All CC levels				
10	6771	16644	16723	25681
20	5823	9313	10024	22964
50	4030	2377	3029	12076
100	1769	753	1033	4909
200	1342	348	538	2201
500	882	124	219	796
1000	583	68	113	411
Total	8158	28203	28203	28203
CC levels 1 – 87				
10	698	1810	1523	3503
20	560	768	610	3205
50	320	79	68	1015
100	138	22	37	178
200	112	11	19	70
500	79	0	4	35
1000	49	0	0	12
Total	1119	3741	3741	3741
Transition from levels $i = 1 - 4$ to $j = 1 - 87$				
10	43	163	93	337
20	31	17	7	329
50	19	2	2	99
100	10	1	2	5
200	8	0	1	2
500	5	0	0	1
1000	2	0	0	1
Total	90	338	338	338

Table 5. Number of transitions in the lower panels of Fig. 7 that differ by more than $\delta = |\Upsilon_{\rm ICFT} - \Upsilon_{\rm BSR}|/\Upsilon_{\rm BSR}$.

δ		Temperature (K)		
(%)	gf	3.2×10^4	1.6×10^5	1.6×10^6
All CC levels				
10	6788	20589	20839	21783
20	5900	14701	15402	17054
50	4055	5339	7195	9459
100	1782	571	736	1402
200	1340	317	460	883
500	910	127	203	462
1000	642	57	97	254
Total	8158	28203	28203	28203
CC levels 1 – 87				
10	747	2215	2073	2206
20	576	1177	1020	1181
50	302	159	177	305
100	121	23	35	66
200	84	15	25	56
500	69	5	13	36
1000	58	0	1	14
Total	1119	3741	3741	3741
Transition from levels $i = 1 - 4$ to $j = 1 - 87$				
10	42	200	126	131
20	30	45	14	27
50	12	5	2	4
100	6	1	2	2
200	4	1	1	2
500	3	0	0	2
1000	2	0	0	0
Total	90	338	338	338

principal source for the differences. For further detail we display in Tables 4 and 5 the number of points in Fig. 2 that deviate by more than a fixed percentage from the diagonal. In both comparisons, DARC or ICFT vs. BSR, the dispersions are similar. They are much smaller for transitions with upper levels up to #87 than for all levels. This comparison, therefore, does not suggest which of the previous works [1, 2] is of better quality. We can only state that both are different and that the principal source for the deviations originates in the target structure.

As discussed in Sect. 2, our target structure description appears to be significantly more accurate than those used in previous works. We cannot, however, state the same about the Υ values. Recall that we had to cut the CC expansion to a size for which we could handle the resulting matrices. It was shown in [35] that cutting the CC expansion can lead to significant errors for transitions to levels above those omitted from the CI expansion. Consequently, we cannot properly assess the accuracy for transitions involving level #88 and above, this time not because of limitations in the target structure as in previous works but due to limitations in the CC expansion.

4.1. Peak abundance temperature

The peak abundance temperature $T_{\rm peak}$ of N^{3+} in collisional plasmas lies around 126000 K [36]. At temperatures close to this, there is overall good agreement between the results from the three calculations for transitions where the CI and CC expansions have essentially converged. Tables 4 and 5 show that for levels below #88, the predictions for approximately 80% of the transitions agree within 20% for all calculations.

The deviations of the results obtained by the ICFT method are found mainly in spin-changing transitions with small spin-orbit mixing in the target. They might be caused by spin-orbit coupling of the colliding electron with the target. This is the only interaction that the ICFT formalism does not account for, in contrast to the Breit-Pauli and the full-relativistic calculations.

4.2. Low temperature

In low-density photo-ionized plasmas, N^{3+} may exist at temperatures much lower than $T_{\rm peak}$. In such a regime the most important contributions to Υ originate from

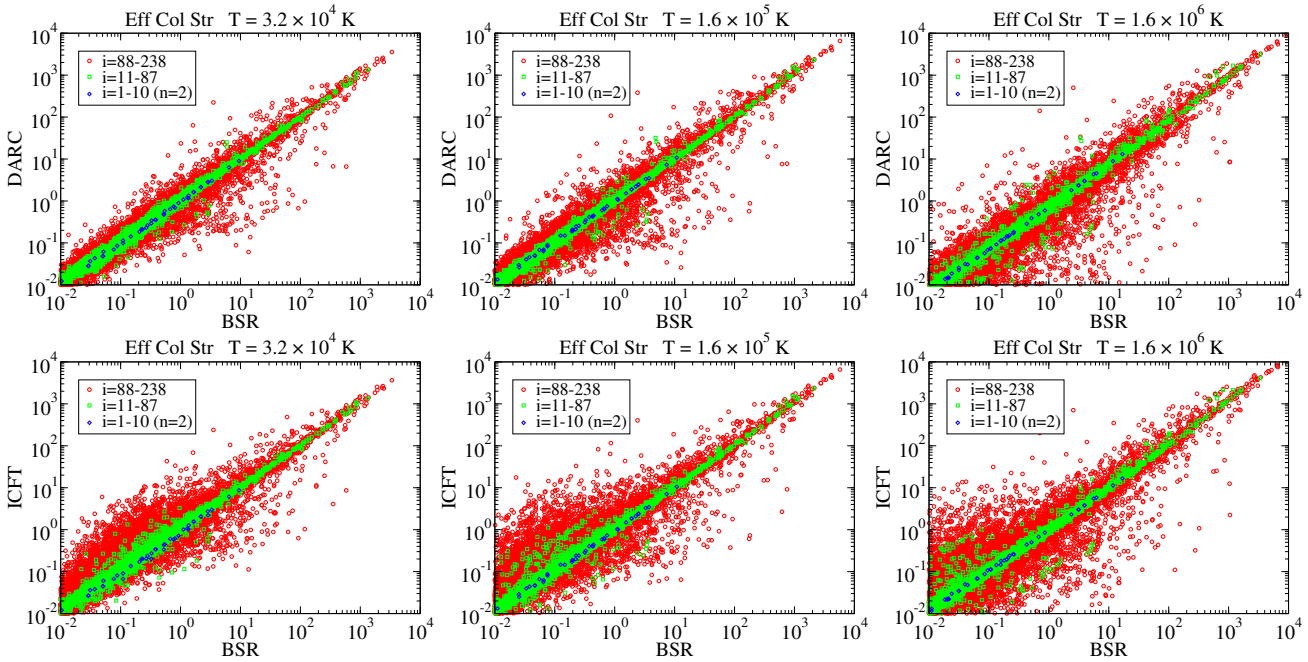

Figure 7. Comparison of effective collision strengths for the present BSR work with DARC [2] (upper panels) and ICFT [1] (lower panels) for three temperatures. Axes and symbols as in Fig. 2.

resonances. The positions of these resonances are directly connected with the energies of the target levels. To generate good-quality results at low temperature, it is important to have the resonances in their correct position and well-resolved in energy. Recall that the present calculation obtains the target energy levels closest to the NIST-recommended values. It is also the one with the finest mesh in the resonance region $10^{-5}z^2$. This suggests that the present work generated the most reliable results in the low-temperature regime.

The results for low temperatures could be improved by adjusting the level energies to the recommended ones. Such operation, however, perturbs the hamiltonian, including the non-diagonal matrix elements and, in turn, may affect the results in the peak-abundance and high-temperature regimes, which are most important for many applications, specifically for collisional plasmas. Usually the low-temperature region is treated individually in studies specially focused on this regime. By analyzing our results in detail, we can confirm that the position of the resonances is the principal cause of disagreement at low temperatures between the BSR and ICFT results for the spin-changing transition 1 – 3 shown in Fig. 6.

4.3. High temperature

The high-energy part of the collision strengths is mostly determined by the infinite energy point, either the collision strength f for dipole-allowed transitions or the Born infinite-energy $\Omega^{\rm B}_{\infty}$ for the forbidden ones. This point depends exclusively on the target structure, i.e., it is independent of the dynamical method used for the collision calculation, including details of the close-coupling expansion. Since the present model produces the most accurate target structure for N^{3+} to date, we expect it to also produce the most accurate results for electron-impact excitation of N^{3+} in the high-temperature region, including the highly-excited states above level #87.

5. Conclusions

The present work sheds new light on the important topic of effects due to the description of the target structure in collision calculations. We have independently obtained electron-impact excitation collision strengths for the N^{3+} ion and carried out a thorough comparison with predictions from previous ICFT and DARC calculations [1, 2]. The close-coupling expansion contained the same number of target states in all calculations. Comparing the results thus directly reveals the influence of the different structure descriptions.

The large differences in the collision strengths from these calculations, seen in some cases, suggest that the target structure is the main source of inaccuracy and uncertainty in these calculations, with the largest effects on transitions involving highly-excited levels. The convergence of the CI expansion is essential for a proper description of the target, and in standard applications of the R-matrix method it can no longer be assessed as one approaches the limit of the CC expansion. An incomplete basis set leaves gaps in the spectrum. This gap may contain several configurations or even entire Rydberg

series, including the continuum. When states in the CI expansion are strongly mixed and some are omitted, their effect on the scattering results can no longer be properly assessed.

Furthermore, one has to consider the usual limitation of the CC expansion in the actual calculation, which is due to the available computational resources. No close-coupling method can claim the validity of its results for target states close to or even above the levels discarded in the CC expansion [35].

It has recently been emphasized that uncertainty estimates for theoretical predictions are essential for their usefulness in practical applications [37]. Even though this is a difficult task in the present work, we believe that the ICFT, DARC, and BSR results are accurate at the 20% level for the majority of the strong transitions up to level #87. Nevertheless, the lack of coupling to the ionization continuum via a sufficient number of pseudo-states in all the present models for the case of interest leaves room for surprises, especially for the weak transitions. For a few levels, the differences in the various predictions reach a factor of two or even more. These differences are, once again, mainly due to the representation of the target structure.

The present work does not support the conjecture of Aggarwal *et al.* [2] that the differences with the results of [1] are due to either the general validity or the practical implementation of the ICFT method. The differences between the present BSR collision strengths and the corresponding ICFT results are approximately the same as those between the BSR and DARC calculations. The only cases where the ICFT method may clearly lead to errors involves weak spin-changing transitions between levels with small spin-orbit mixing, which can be strongly influenced through the spin-orbit coupling with the incoming electron. This mechanism is not considered by the ICFT method. However, such weak transitions are in general not relevant for plasma modeling, certainly not in collisional plasmas.

Due to the superior target structure generated in the present work, we believe that the present results are the currently best for electron collisions with N^{3+}. The differences between the BSR and the DARC / ICFT results may in fact serve as an uncertainty estimate for the available excitation rates. We are confident regarding the accuracy of the collision strengths for strong transitions among the low-lying levels up #87 in the N^{3+} spectrum, while the results for transitions to the higher-lying states remain questionable, especially for the weak intercombination transitions. This situation is typical for many existing datasets and calls for further detailed consideration.

Acknowledgments

This work was supported by the United States National Science Foundation through grant No. PHY-1520970. The numerical calculations were performed on STAMPEDE at the Texas Advanced Computing Center. They were made possible by the XSEDE allocation No. PHY-090031.

References

[1] Fernández-Menchero L, Del Zanna G and Badnell N R 2014 *Astron. Astroph.* **566** A104
[2] Aggarwal K M, Keenan F P and Lawson K D 2016 *Mon. Not. R. Astr. Soc.* **461** 3997
[3] Burke P G 2011 *R-Matrix of Atomic Collisions: Application to Atomic, Molecular, and Optical Processes* (Springer-Verlag, New-York)
[4] Berrington K A, Eissner W B and Norrington P H 1995 *Comp. Phys. Comm.* **92** 290
[5] `http://amdpp.phys.strath.ac.uk/rmatrix/`
[6] `http://amdpp.phys.strath.ac.uk/rmatrix/ser/darc/`
[7] Berrington K A, Ballance C P, Griffin D C, and Badnell N R 2005 *J. Phys. B: At. Mol. Opt. Phys.* **38** 1667
[8] Zatsarinny O 2006 *Comp. Phys. Comm.* **174** 273
[9] Zatsarinny O and Bartschat K 2013 *J. Phys. B: At. Mol. Opt. Phys.* **46** 112001
[10] Tayal S S and Zatsarinny O 2014 *Astroph. J.* **788** 24
[11] Tayal S S and Zatsarinny O 2011 *Astroph. J.* **743** 206
[12] Griffin D C, Badnell N R and Pindzola M S 1998 *J. Phys. B: At. Mol. Opt. Phys.* **31** 3713
[13] Fernández-Menchero L, Del Zanna G and Badnell N R 2015 *Mon. Not. R. Astr. Soc.* **450** 4174
[14] Del Zanna G, Badnell N R, Fernández-Menchero L, Liang G T, Mason H E and Storey P J 2015 *Mon. Not. R. Astr. Soc.* **454** 2909
[15] Aggarwal K M and Keenan F P 2015 *Mon. Not. R. Astr. Soc.* **447** 3849
[16] Aggarwal K M and Keenan F P 2015 *Mon. Not. R. Astr. Soc.* **450** 1151
[17] Aggarwal K M and Keenan F P 2014 *Mon. Not. R. Astr. Soc.* **445** 2015
[18] Zatsarinny O and Fischer C F 2002 *J. Phys. B: At. Mol. Opt. Phys.* **35** 4669
[19] Zatsarinny O and Froese-Fischer C 2009 *Comp. Phys. Comm.* **180** 2041
[20] Zatsarinny O, Bartschat K, Fursa D V and Bray I 2016 *J. Phys. B: At. Mol. Opt. Phys.* in press
[21] Badnell N R 2011 *Comp. Phys. Comm.* **182** 1528
[22] Dyall K G, Grant I P, Johnson C T, Parpia F A and Plummer E P 1989 *Comp. Phys. Comm.* **55** 425
[23] Parpia F A, Fischer C F and Grant I P 1996 *Comp. Phys. Comm.* **94** 249
[24] Moore C E 1993 *Tables of Spectra of Hydrogen, Carbon, Nitrogen and Oxygen Atoms and Ions* CRC Series in Evaluated Data in Atomic Physics (CRC Press) ISBN 978-0849374203; online available at `http://physics.nist.gov/asd` [2016, Nov. 10]. Kramida A, Ralchenko Yu, Reader J, and NIST ASD Team (2015). NIST Atomic Spectra Database (ver. 5.3), National Institute of Standards and Technology, Gaithersburg, MD.
[25] Froese-Fischer C and Tachiev G 2004 *At. Data Nucl. Data Tables* **87** 1
[26] Engström L, Denne B, Ekberg J O, Jones K W, Jupén C, Litzén U, Weng Tai Meng, Trigueiros A and Martinson I 1981 *Phys. Scr.* **24** 551
[27] Doerfert J, Träbert E and Wolf A 1996 *Hyperfine Interactions* **99**
[28] Chen, M-K 1999 *Phys. Scr.* **T80** 485
[29] Ceyzeriat P, Denis A, Desesquelles J, Druetta M and Poulizac M 1970 *Nuclear Instruments and Methods* **90** 103

[30] Buttle P J A 1967 *Phys. Rev.* **160** 719
[31] Burgess A 1974 *J. Phys. B: At. Mol. Phys.* **7** L364
[32] Badnell N R and Griffin D C 2001 *J. Phys. B: At. Mol. Opt. Phys.* **34** 681
[33] Berrington K A, Burke P G, Butler K, Seaton M J, Storey P J, Taylor K T and Yan Y 1987 *J. Phys. B: At. Mol. Phys.* **20** 6379
[34] Badnell N R and Griffin D C 1999 *J. Phys. B: At. Mol. Opt. Phys.* **32** 2267
[35] Fernández-Menchero L, Giunta A S, Del Zanna G and Badnell N R 2016 *J. Phys. B: At. Mol. Opt. Phys.* **49** 085203
[36] Mazzotta P, Mazzitelli G, Colafrancesco S and Vittorio N 1998 *Astron. Astroph. Suppl. Ser.* **133** 403
[37] Chung H-K, Braams B J, Bartschat K, Császár A G, Drake G W F, Kirchner T, Kokoouline V, and Tennyson J 2016 *J. Phys. D: Appl. Phys.* **49** 363002